

Sterically Governed Selectivity in Palladium-Assisted Allylic Alkylation

Jonatan Kleimark,[†] Charlotte Johansson,[†] Susanne Olsson,[†] Mikael Håkansson,[†]
Sverker Hansson,[‡] Björn Åkermark,[§] and Per-Ola Norrby^{*†}

[†]Department of Chemistry, University of Gothenburg, Kemigården 4, SE-412 96 Göteborg, Sweden,
[‡]Astrazeneca, SE-151 85 Södertälje, Sweden, and [§]Arrhenius Laboratory, Department of Organic Chemistry,
Stockholm University, SE-106 91 Stockholm, Sweden

Received July 26, 2010

The selectivity in the Pd-assisted allylic alkylation has been investigated in a system with a ligand tethered to the allylic moiety. Isolation of (η^3 -allyl)Pd complexes and stoichiometric reaction with malonate nucleophiles allowed separation of various factors influencing the regioselectivity in a system that cannot undergo apparent rotation. Unexpectedly, trans effects were found to have only a minor influence on the selectivity, whereas changing the tether length could shift the preference from favored internal to dominant terminal attack. DFT-assisted analysis revealed that the dominant selectivity-determining factors are the forced rotation of the allylic moiety and an important steric repulsion from a *syn*-alkyl substituent.

Introduction

Palladium-assisted allylation is a standard reaction in the toolbox of organic chemistry. The reaction is usually stereo-specific, can be run under mild conditions with a large range of nucleophiles, and tolerates a wide range of functional groups.¹ When employing stabilized carbanion nucleophiles such as malonates, the reaction is known as allylic alkylation, or the Tsuji–Trost reaction.² The asymmetric version of this reaction is a popular method for creating new chiral centers while at the same time extending the carbon framework.³ The mechanism of the title reaction involves initial oxidative addition of a Pd⁰ complex to an allylic substrate (e.g., acetate) to form an intermediate (η^3 -allyl)Pd complex, which is attacked by a nucleophile to produce the final product with loss of Pd⁰, Scheme 1. Both steps most commonly proceed with inversion, giving overall retention.

Asymmetric versions of the Tsuji–Trost reaction are frequently applied to substrates that yield symmetrically substituted (η^3 -allyl)Pd intermediates, such as cycloalkenyl or 1,3-diphenylallyl complexes.³ In such cases, enantioselectivity is determined by the regioselectivity of the nucleophilic attack.⁴ In unsymmetric cases, like the monosubstituted (η^3 -allyl)Pd complex depicted in Scheme 1, the regioselectivity is

known to be sensitive to many factors, such as steric and electronic influences from the substrate substituents,⁵ regiochemical memory of the position of the leaving group,⁶ the preferred configuration^{7,8} and dynamic exchange in the (η^3 -allyl)Pd intermediate,⁹ the nucleophile,¹⁰ and the nature of the ligands.^{4,11,12} For example, it could be shown that *syn*-substituted (η^3 -allyl)Pd complexes have a strong preference for terminal attack, whereas the corresponding *anti*-substituted complexes gave product mixtures with significant amounts of internal attack.^{7,8} The latter has important implications for the possibilities of inducing asymmetry, since internal attack produces a new stereocenter. Ligand-induced distortions of the intermediate have also been shown to have a strong effect on the regiochemical preference in the nucleophilic attack.¹³ However, despite numerous advances we are still far from a complete understanding of the behavior of (η^3 -allyl)Pd complexes. For selected substrates, we can achieve very high selectivities, but a general control of the regiochemistry in Pd-assisted allylic alkylation still eludes us.

*To whom correspondence should be addressed. E-mail: pon@chem.gu.se.

(1) (a) Hartwig, J. F. *Organotransition Metal Chemistry—From Bonding to Catalysis*; University Science Books: Sausalito, CA, 2010. (b) Tsuji, J. *Palladium Reagents and Catalysts: Innovations in Organic Synthesis*; Wiley: Chichester, UK, 1997.

(2) (a) Trost, B. M.; Crawley, M. L. *Chem. Rev.* **2003**, *103*, 2921–2943. (b) Tsuji, J. In *Handbook of Organopalladium Chemistry for Organic Synthesis*, Vol. 2; Negishi, E.-i., Ed.; Wiley: New York, 2002.

(3) (a) Trost, B. M.; Lee, C. In *Catalytic Asymmetric Synthesis*, 2nd ed.; Ojima, I., Ed.; Wiley-VCH: New York, 2000; pp 593–649. (b) Pfaltz, A.; Lautens, M. In *Comprehensive Asymmetric Catalysis*; Jacobsen, E. N.; Pfaltz, A.; Yamamoto, H., Eds.; Springer: Heidelberg, 1999; pp 833–886.

(4) Trost, B. M.; Toste, F. D. *J. Am. Chem. Soc.* **1999**, *121*, 4545–4554.

(5) (a) Szabó, K. J. *Chem. Soc. Rev.* **2001**, *30*, 136–143. (b) Branchadell, V.; Moreno-Mañas, M.; Pajuelo, F.; Pleixats, R. *Organometallics* **1999**, *18*, 4934–4941.

(6) Lloyd-Jones, G. C.; Stephen, S. C. *Chem. Eur. J.* **1998**, *4*, 2539–2549.

(7) Sjögren, M.; Hansson, S.; Norrby, P.-O.; Åkermark, B.; Cucciolito, M. E.; Vitagliano, A. *Organometallics* **1992**, *11*, 3954–3964.

(8) Fristrup, P.; Jensen, T.; Hoppe, J.; Norrby, P.-O. *Chem. Eur. J.* **2006**, *12*, 5352–5360.

(9) Hansson, S.; Norrby, P.-O.; Sjögren, M.; Åkermark, B.; Cucciolito, M. E.; Giordano, F.; Vitagliano, A. *Organometallics* **1993**, *12*, 4940–4948.

(10) Kazmaier, U.; Stolz, D.; Kraemer, K.; Zumpfe, F. L. *Chem. Eur. J.* **2008**, *14*, 1322–1329.

(11) Lu, Z.; Ma, S. *Angew Chem., Int. Ed.* **2008**, *47*, 258–297.

(12) (a) Kranenburg, M.; Kamer, P. C. J.; van Leeuwen, P. W. N. M. *Eur. J. Inorg. Chem.* **1998**, 25–27. (b) Frölander, A.; Lutsenko, S.; Privalov, T.; Moberg, C. *J. Org. Chem.* **2005**, *70*, 9882–9891. (c) Hayashi, T.; Yamamoto, A.; Ito, Y.; Nishioka, E.; Miura, H.; Yanagi, K. *J. Am. Chem. Soc.* **1989**, *111*, 6301–6311.

(13) Oslo, J. D.; Åkermark, B.; Helquist, P.; Norrby, P.-O. *Organometallics* **1997**, *16*, 3015.

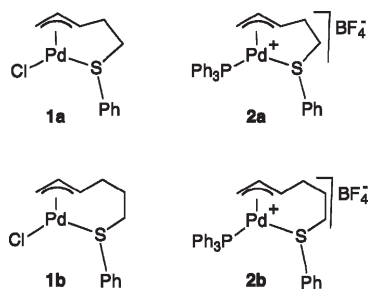
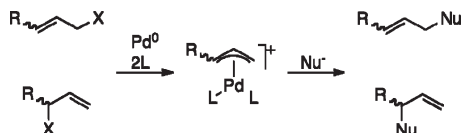


Figure 1. (η^3 -allyl)Pd complexes with a tethered sulfide ligand.

Scheme 1. Possible Products in a Pd-Catalyzed Allylic Alkylation



It has long been recognized that ligands on Pd can influence the regioselectivity of nucleophilic attack. In particular, the large trans effect of phosphorus will enhance reactivity on the allylic terminus trans to any phosphine.¹⁴ This phenomenon was utilized in a breakthrough in asymmetric allylic alkylation in the early 1990s, when three groups independently introduced the phosphino-oxazoline class of ligands now known as PHOX.¹⁵ Several other groups developed bidentate ligands with two different coordinating heteroatoms,¹¹ mostly phosphorus and nitrogen, but also, for example, sulfur.¹⁶

Quantifying the magnitude of the trans effect in the Tsuji–Troost reaction and separating it from steric influences is not a trivial task. A lower limit was demonstrated in a system where the difference in trans effect between phosphines and chloride gave regioselectivity up to 40%,¹⁷ but interpretation is complicated by the many dynamic processes available to (η^3 -allyl)Pd complexes, most of which are accelerated by the presence of chloride.¹⁸ More recently, it was shown that, in the presence of a simple P,N-ligand, the regioselectivity that would be expected from the known difference in trans effect between P and N was almost completely absent. This surprising result was attributed to very efficient apparent rotation in the cationic (η^3 -allyl)Pd intermediate.¹⁹ Thus, accurate measurement of the balance between sterics and trans effects in the Tsuji–Troost reaction requires negation of the apparent rotation. This can be achieved by tethering one of the ligands to the allylic moiety. We have performed preliminary computational and experimental studies on systems with a tethered sulfide ligand (Figure 1).²⁰

(14) Åkermark, B.; Zetterberg, K.; Hansson, S.; Krakenberger, B.; Vitagliano, A. *J. Organomet. Chem.* **1987**, *335*, 133–142.

(15) (a) von Matt, P.; Pfaltz, A. *Angew. Chem., Int. Ed. Engl.* **1993**, *32*, 566–569. (b) Sprinz, J.; Helmchen, G. *Tetrahedron Lett.* **1993**, *34*, 1769–1773. (c) Allen, J. V.; Coote, S. J.; Dawson, G. J.; Frost, C. G.; Martin, C. J.; Williams, J. M. J. *J. Chem. Soc., Perkin Trans. 1* **1994**, 2065–2072.

(16) (a) Pellissier, H. *Chiral Sulfur Ligands: Asymmetric Catalysis*; RSC: Cambridge, 2009. (b) Evans, D. A.; Campos, K. R.; Tedrow, J. S.; Michael, F. E.; Gagné, M. R. *J. Am. Chem. Soc.* **2000**, *122*, 7905–7920.

(17) Svensen, N.; Fristrup, P.; Tanner, D.; Norrby, P.-O. *Adv. Synth. Catal.* **2007**, *349*, 2631–2640.

(18) Vrieze, K. In *Dynamic Nuclear Magnetic Resonance Spectroscopy*; Jackman, L. M., Cotton, F. A., Eds.; Academic Press: New York, 1975.

(19) Johansson, C.; Lloyd-Jones, G. C.; Norrby, P.-O. *Tetrahedron: Asymmetry* **2010**, *21*, 1585–1592.

(20) (a) Norrby, P.-O.; Åkermark, B.; Häffner, F.; Hansson, S.; Blomberg, M. *J. Am. Chem. Soc.* **1993**, *115*, 4859. (b) Norrby, P.-O. Ph. D. Thesis, KTH, Stockholm, 1992.

However, the results were hard to interpret. It was known that the regioselectivity could be strongly influenced by the *syn*–*anti* equilibrium in the (η^3 -allyl)Pd intermediate,^{7,8} but we could not at that time elucidate the preferred structure of the tethered intermediate. Yoshida and co-workers have investigated the effect of a removable pyridine tether,²¹ but they did not perform a detailed analysis of the reasons for the good regioselectivity. Krafft and co-workers studied catalytic systems with a range of tethered ligands, including alkenes²² and sulfides,²³ but they did not ascertain which ligands were bound to Pd during the nucleophilic attack. Some of their results indicate that, in a catalytic system, the tethered heteroatom interacts with the approaching nucleophile, not Pd. For the purpose of investigating the trans effect from the ligands, we must ascertain the coordination geometry, which is most easily done in stoichiometric reactions.

We want to employ the systems depicted in Figure 1 in order to quantify the importance of the trans effect relative to the steric bias inherent in a monosubstituted η^3 -allyl electrophile. To this end, we have isolated the complexes and studied their reaction with a nucleophile. Further, the complexes have been studied both in solid state and in solution to confirm the proposed structures. We have also performed a computational study of the complexes themselves as well as their reactivity, to elucidate the source of the observed selectivities in the allylic alkylation reaction.

Experimental Results

Alkenes with tethered sulfide ligands, precursors to the complexes in Figure 1, were synthesized from the corresponding bromides (Scheme 2). Neutral (η^3 -allyl)Pd complexes **1** were prepared by reaction of the alkenes with palladium trifluoroacetate and a base, followed by anion exchange with lithium chloride. To prepare the cationic (η^3 -allyl)Pd complexes **2**, the neutral complexes were treated with triphenyl phosphine and silver tetrafluoroborate, precipitating silver chloride. Complexes with a dimethylene tether, **1a** and **2a**, were obtained in moderate to high yield. Synthesis of complexes with a trimethylene tether was more problematic and frequently yielded a byproduct, **3** (X = Cl or PPh₃), from an apparent hydride shift.

The preferred regioselectivity on nucleophilic attack for all four complexes (**1a,b** and **2a,b**) was tested in a standard alkylation reaction using sodium dimethyl malonate as nucleophile (Scheme 3). Analyses by GC-MS and ¹H NMR showed that each complex gave rise to two products: the linear product, **4**, from the terminal attack, and the branched product, **5**, from the internal attack. The product distribution in each case is shown in Table 1.

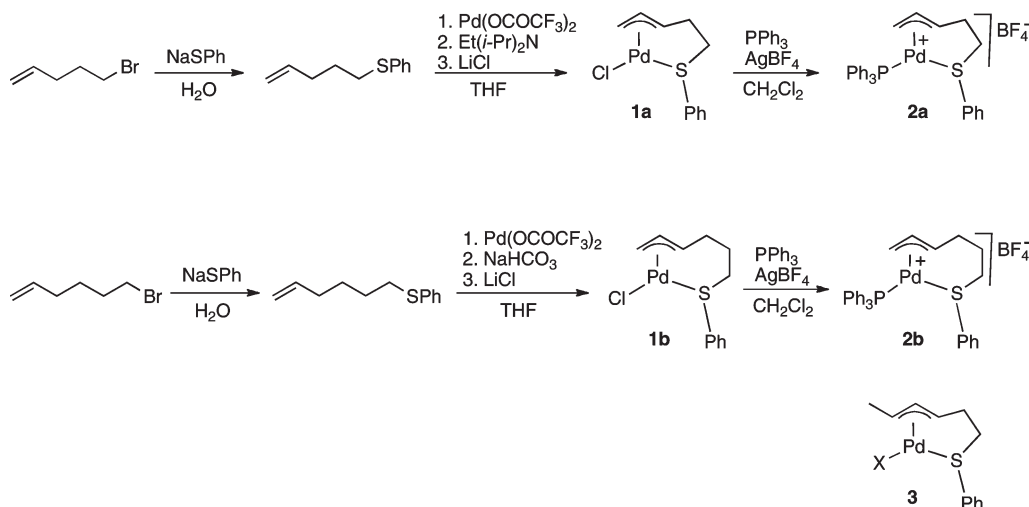
Looking first at the cationic phosphine complexes **2**, we can see that the regioselectivity is determined by the geometry of the allylic moiety, not by the nature of the ligands. The selectivity shifts from a preference for internal attack with the shorter tether (**2a**) to a preference for terminal attack in the homologue with an additional methylene unit (**2b**). Thus, it is clear that the steric preference inherent in the allylic moiety is strong relative to the influence from the trans effect difference. However, the kinetic trans effect can be detected by an isodesmic comparison of the chloride and phosphine complexes. When going from

(21) Itami, K.; Koike, T.; Yoshida, J.-I. *J. Am. Chem. Soc.* **2001**, *123*, 6957–6958.

(22) Krafft, M. E.; Sugiura, M.; Abboud, K. A. *J. Am. Chem. Soc.* **2001**, *123*, 9174–9175.

(23) (a) Krafft, M. E.; Fu, Z.; Procter, M. J.; Wilson, A. M.; Hirotsawa, C. *Pure Appl. Chem.* **1998**, *70*, 1083–1090. (b) Krafft, M. E.; Wilson, A. M.; Fu, Z.; Procter, M. J.; Dasse, O. A. *J. Org. Chem.* **1998**, *63*, 1748–1749.

Scheme 2. Synthetic Route to 1,2a and 1,2b



Scheme 3. Regioisomeric Products Formed in the Reaction with Sodium Dimethyl Malonate

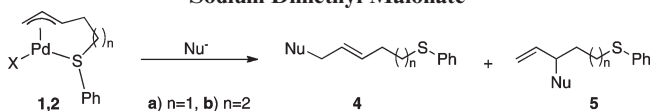


Table 1. Product Distribution from Reactions in Scheme 3

complex	ligand X	tether length	linear 4 (%)	branched 5 (%)
1a	Cl	2	40	60
1b	Cl	3	80	20
2a	PPh ₃	2	20	80
2b	PPh ₃	3	80	20

chloride to phosphine, the amount of branched product increases when utilizing the smaller complexes, showing that nucleophilic attack trans to phosphorus is more favorable than attack trans to chloride, in agreement with known differences in trans effect of these two ligands.²⁴ We also note that the results obtained by Krafft and co-workers in a catalytic system is the same as what we see for the isolated complex **2a**,²³ indicating that the tethered ligand is coordinated to Pd during the reaction. Further, in their study they reported that using Pd(PPh₃)₄ gave rise to mixed results, compared to the results when applying (η^3 -allyl)PdPPh₃Cl. The reason for this might be that the excess PPh₃ replaces the sulfide tether. To test this assumption, we wanted to perform the reaction with a nucleophile under conditions where the tethered sulfide does *not* coordinate to the palladium. Since the dominant factor leading to coordination of the sulfide is a chelate effect, it can be negated by utilization of a stronger, chelate-assisted ligand, a phosphine. Since the complex with the shorter tether seems to be under strain, it is even possible that a sufficiently strong ligand can displace sulfur even without chelate assistance. With this in mind, we reacted complex **1a** with two different competing ligands, either one equivalent of dppe (1,2-(diphenylphosphino)ethane) or an excess of PPh₃, followed by treatment with the standard nucleophile, the sodium salt of dimethyl malonate. The results, depicted in Scheme 4, clearly show that both phosphine systems are able to displace the tethered sulfide. In the absence of tethering and differential trans influences, the selectivity becomes more similar to that of the system using the longer tether (Table 1, **1b**;

80:20). The selectivities now resemble the ones obtained with isolated *syn*-alkyl complexes,^{7,25} as well as with the *syn*-component in equilibrating *syn-anti* mixtures.⁸ We also note that the results shown in Scheme 4 disprove the proposal of Krafft and co-workers that the uncomplexed sulfide should be able to direct the incoming nucleophile to the internal position.²³

Several factors have been shown to influence the regioselectivity of attack on unsymmetrically substituted (η^3 -allyl)Pd moieties. In general, a monoalkyl substituent will shift the reactivity to the terminal position, but the preference for internal attack can be increased if the substituent is oriented in the *anti*-position.^{7,8} Thus, the current results could be rationalized if the shorter tether induces a preference for an *anti*-substituted η^3 -allyl. However, preliminary results obtained with a specially designed molecular mechanics force field²⁰ indicate that the *syn*-configuration should be preferred for both tethers, and in particular for the shorter one. Thus, an explanation based on *syn-anti* equilibration seems unlikely. However, to be sure that the *syn*-configuration was preferred also in the experimental study, the solid state of the complexes **1a,b** and **2a,b** (Figure 1) were studied by X-ray diffraction, and the structures in solution were studied by NMR spectroscopy.

Structure in Solution. All four complexes (**1a,b** and **2a,b**) were fully characterized by 1D- and 2D-¹H NMR spectroscopy. The ¹H NMR spectra of the complexes were assigned by using COSY experiments, and the structure was assigned by measuring the coupling constants between the protons in the allylic moiety. Primarily, the coupling constant between H2 and H3 is informative for determining whether the complex is the *syn*- or the *anti*-isomer. In the *anti*-isomer, where the H3 is in *syn*-position, the coupling constant is in the range 6.5–8 Hz, and in the *syn*-isomer, where the H3 is in *anti*-position, the coupling constant is in the range 11.5–14 Hz.²⁶ In all complexes, **1a,b** and **2a,b**, the coupling constant between H2 and H3 was in the range 11–13 Hz, which confirmed that all detectable complexes were *syn*-isomers in solution.

Crystallographic Study. In the solid state all four complexes feature palladium in a distorted square-planar coordination geometry, with Pd surrounded by the sulfur atom and the allylic moiety of the tethered ligand and either chloride or triphenylphosphine. In **1a** and **1b** the anionic chloride is coordinated to Pd, forming a neutral complex, whereas in **2a** and **2b** the neutral phosphine ligand makes the complexes cationic with noncoordinating BF₄ as counterion. In the crystal structure of **2a** and **2b** the BF₄'s are disordered, and this results in raised *R* values and thus poorer quality for the overall structure determination especially for structure **1b**. The conformations of the two- and three-methylene-tethered complexes

(24) Coe, B. J.; Glenwright, S. J. *Coord. Chem. Rev.* **2000**, *203*, 5–80.(25) Sjögren, M.; Hansson, S.; Åkermark, B.; Vitagliano, A. *Organometallics* **1994**, *13*, 1963–1971.(26) Åkermark, B.; Krakenberger, B.; Hansson, S.; Vitagliano, A. *Organometallics* **1987**, *6*, 620–628.

Scheme 4. Selectivities with and without Coordination of the Tethered Sulfide Ligand

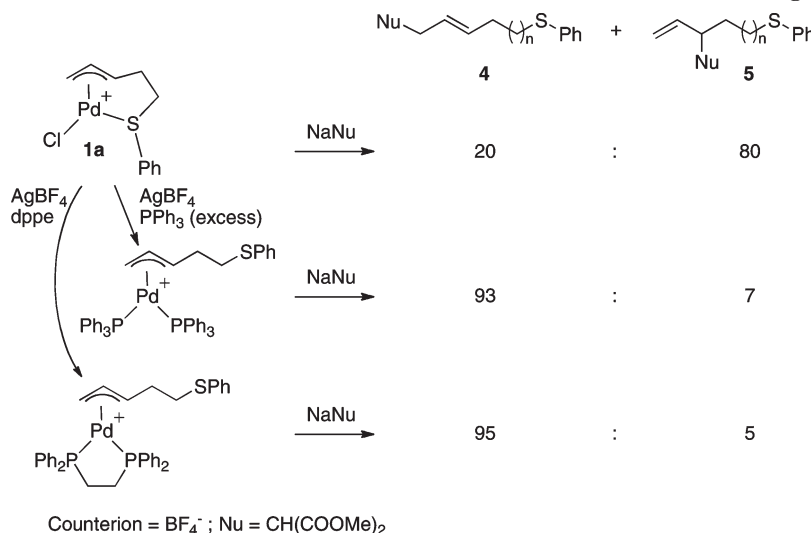


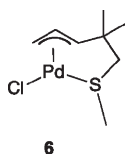
Table 2. Crystal and Refinement Data for 1a,b and 2a,b

	[PdC ₁₁ H ₁₃ ClS]	[PdC ₁₂ H ₁₅ ClS]	[PdC ₂₉ H ₂₈ PS][BF ₄]	[PdC ₃₀ H ₃₀ PS][BF ₄]
formula	1a PdC ₁₁ H ₁₃ ClS	1b PdC ₁₂ H ₁₅ ClS	2a PdC ₂₉ H ₂₈ BF ₄ PS	2b PdC ₃₀ H ₃₀ BF ₄ PS
<i>M</i>	319.12	333.15	632.75	646.78
space group	<i>Pcab</i>	<i>P2₁/c</i>	<i>P2₁/n</i>	<i>Cc</i>
<i>a</i> /Å	7.7780(14)	9.250(2)	14.315(3)	14.005(4)
<i>b</i> /Å	15.665(2)	9.137(2)	9.8835(19)	13.835(3)
<i>c</i> /Å	19.090(3)	15.844(4)	20.117(4)	15.730(5)
α /deg	90	90	90	90
β /deg	90	102.702(9)	102.401(7)	107.523(9)
γ /deg	90	90	90	90
<i>V</i> /Å ³	2326.0(6)	1306.4(6)	2779.8(10)	2906.4(14)
<i>Z</i>	8	4	4	4
<i>D_c</i> /cm ⁻³	1.823	1.694	1.512	1.478
μ (Mo K α)/mm ⁻¹	1.962	1.751	0.844	0.809
<i>T</i> /K	293(2)	293(2)	293(2)	293(2)
cryst size/mm	0.25 × 0.25 × 0.20	0.25 × 0.25 × 0.20	0.30 × 0.20 × 0.05	0.20 × 0.20 × 0.10
no. of rflns collected	14 306	8365	17 965	9518
no. of unique rflns (<i>R</i> _{int})	2096 (0.0325)	2365 (0.0325)	5083 (0.0642)	4999 (0.0366)
GOF on <i>F</i> ²	1.062	1.137	1.250	1.076
final <i>R</i> 1(<i>F</i>) ^a (<i>I</i> > 2 σ (<i>I</i>)/w <i>R</i> 2(<i>F</i> ²) ^b)	0.0358/0.0848	0.0490/0.1072	0.1020/0.1462	0.0442/0.0951
<i>R</i> 1 ^a /w <i>R</i> 2(<i>F</i> ²) ^b (all data)	0.0379/0.0865	0.0560/0.1111	0.1214/0.1533	0.0532/0.0994

$$^a R1(F) = \sum(|F_o| - |F_c|) / \sum |F_o|. \quad ^b wR2(F^2) = \{ \sum [w(F_o^2 - F_c^2)^2] / \sum [w(F_o^2)^2] \}^{1/2}.$$

respectively are very similar, and all consist of *syn*-isomers in the solid state. A summary of the crystal and refinement data can be found in Table 2.

The crystal structure of **1a** (Figure 2) is similar to the structure of the previously reported chloro(*syn*-4,4-dimethyl-5-methylthiopent-(1-3- η)-enyl)palladium, **6**.²⁷ The phenyl substituent on sulfur in **1a** makes the Pd–S–C6 angle in **1a** (119.6°) larger than the Pd–S–Me angle in **6** (110.4°). The crystal structure of **2a** mainly differs from **1a** in the rotation of the phenyl group on sulfur, a low-energy distortion that will be determined primarily by nonbonded interactions in the solid state.



The structures with a three-carbon tether chain, **1b** and **2b** (Figure 3), are quite similar to their homologues **1a** and **2a**. The methylene

chains will adopt *gauche* geometries, which gives the result that the sulfur phenyl orientations differ between the two tether geometries. Sulfur is stereogenic in the complexes, and structure **2b** has an inverted sulfur stereochemistry compared to the other three complexes. Again, the inversion at sulfur is a low-energy process, and the preferred geometry is most probably determined by interactions with the phosphine phenyl groups as well as with neighboring moieties in the crystal. We note that, with the longer tether, the Pd–C3 bond becomes slightly longer, and the *syn* substituent is closer to the plane of the allyl moiety, indicating a less strained structure.

In order to further elucidate the source of the anomalous selectivity, we turned to a computational study, employing DFT methods that have previously been shown to give good predictivity for Pd-assisted allylic alkylation.^{19,28}

Computational Results

In our computational studies, the complete conformational and configurational space of all structures were investigated

(27) McCrindle, R.; Alyea, E. C.; Ferguson, G.; Dias, S. A.; McAlees, A. J.; Parvez, M. *J. Chem. Soc., Dalton Trans.* **1980**, 137–144.

(28) (a) Butts, C. P.; Filali, E.; Lloyd-Jones, G. C.; Norrby, P.-O.; Sale, D. A.; Schramm, Y. *J. Am. Chem. Soc.* **2009**, *131*, 9945–9957. (b) Fristrup, P.; Ahlquist, M.; Tanner, D.; Norrby, P.-O. *J. Phys. Chem.* **2008**, *112*, 12862–12867.

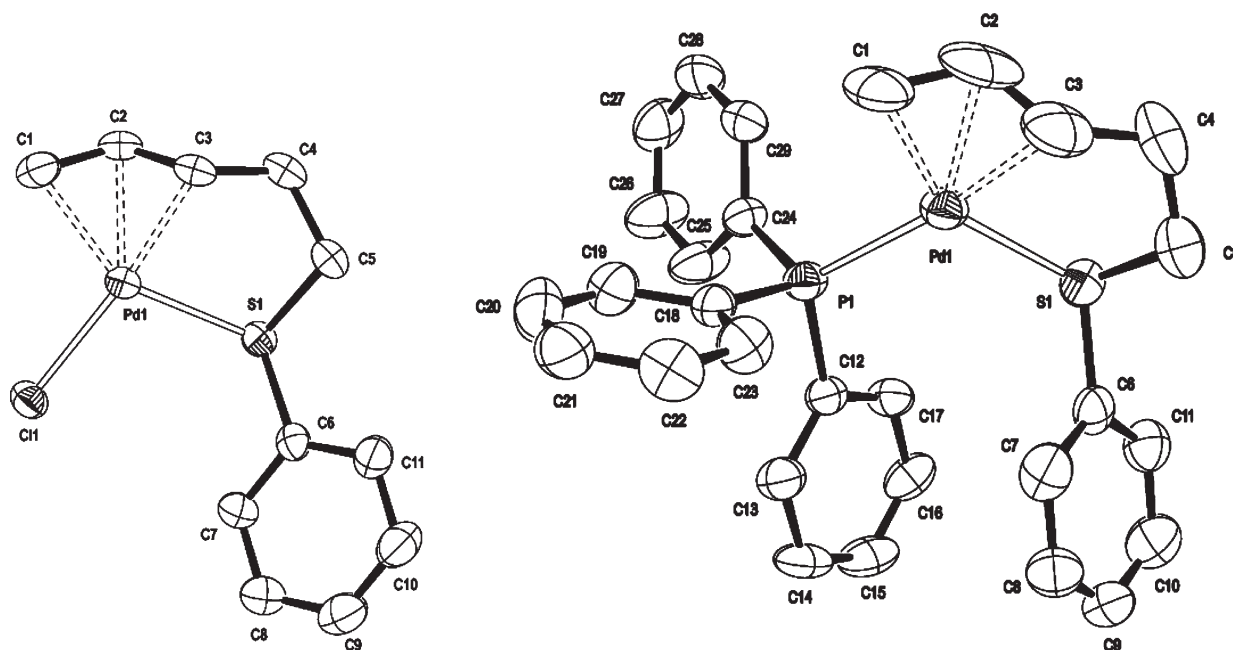


Figure 2. Molecular structure of **1a** and **2a**. Thermal ellipsoids enclose 50% probability. All hydrogen atoms and the disordered BF_4 anion in **2a** have been omitted for clarity.

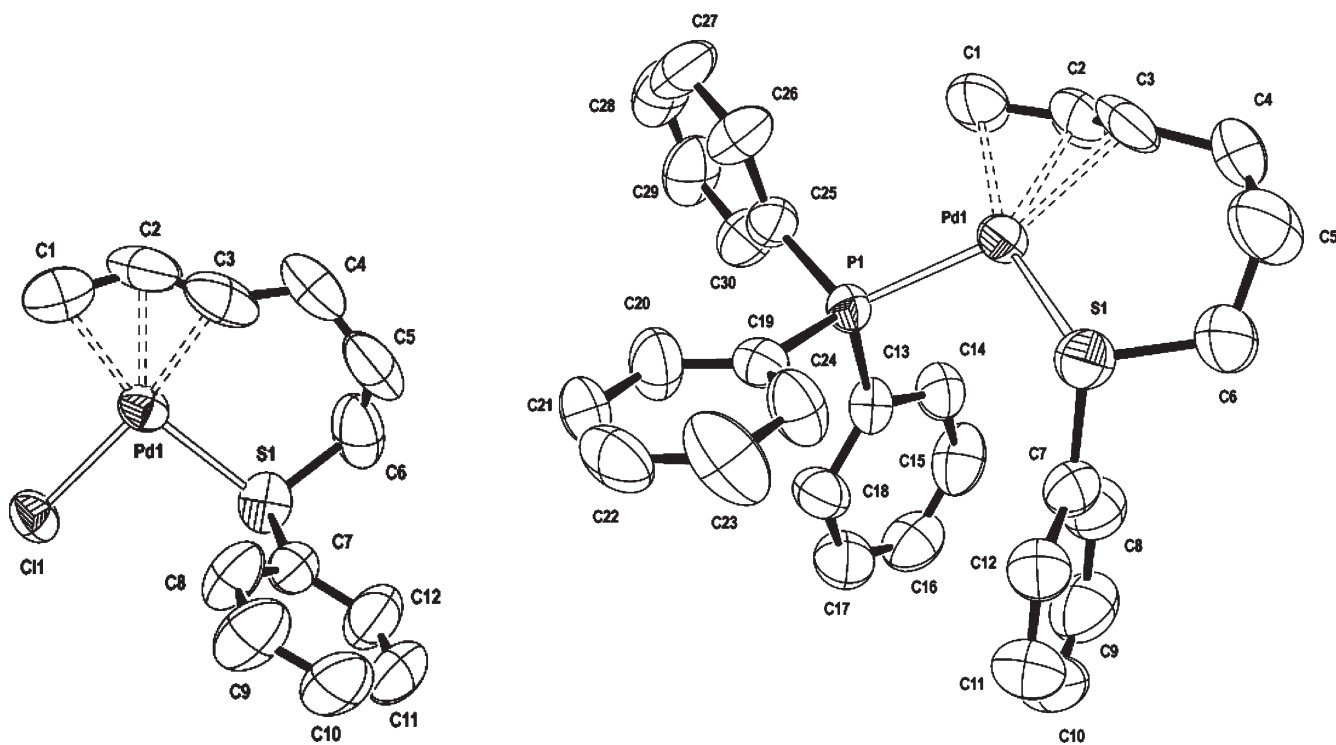


Figure 3. Molecular structures of **1b** and **2b**. Thermal ellipsoids enclose 50% probability. All hydrogen atoms and the disordered BF_4 anion in **2b** have been omitted for clarity.

using a molecular mechanics force field specifically designed for complexes like **1**²⁰ and modified to fit the known structure of **6**.²⁷ All low-energy structures were reoptimized with DFT and used as starting points for transition state searches, as outlined in the Computational Methods section, *vide infra*.

To validate the selected DFT method for $(\eta^3\text{-allyl})$ palladium complexes with a Pd–S bond, the ability to reproduce the known X-ray structure **6**²⁷ was tested. Overlaying all non-hydrogen atoms of the X-ray and DFT-optimized structure gave a root-mean-square (rms) deviation of 0.0531 Å. Almost

all of the error originates from the Pd–S bond, which is too long by approximately 0.1 Å in the DFT structure. This is a systematic error that will occur in all our calculated structures. We can therefore expect error cancellation when comparing related structures.

Investigating the chloride complexes by molecular mechanics, eight geometrical isomers of complex **1a** and 12 of complex **1b** could be located, including both *syn*- and *anti*-isomers. All isomers were reoptimized at the DFT level. The *anti*-isomers were deemed unimportant due to their high energy, at least

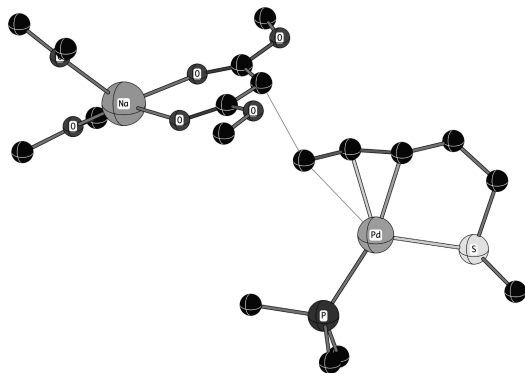


Figure 4. Transition state for terminal attack on complex **2a**. Hydrogen atoms and most of the phenyl moieties were included in the calculation but are hidden for clarity.

18 kJ/mol above the best *syn*-complex. For the *syn*-isomers of the complexes, each tether length showed a strong preference for one ring conformation, displaying the alternating *gauche* conformations generally found in chair cyclohexanes, as well as in the previously reported X-ray structure of **6**. For each complex (**1a** and **1b**), two low-energy conformations were selected for further studies, differing only in the orientation of the sulfide phenyl substituent. The resulting four structures were used as starting points for optimization of the corresponding cationic phosphine complexes (**2a** and **2b**), for which no molecular mechanics parameters were available. The optimized structures were then employed in a transition state search with sodium dimethyl malonate as the nucleophile. The coordination sphere of the Na atom was solvated with two explicit ether molecules (Me_2O) to avoid nonphysical interactions with the substrate. This small model, used together with standard continuum solvation, has previously been used successfully to represent THF coordination.²⁸ For each approach vector of the nucleophile, at least three rotameric forms were tested, but the discussion below is based on the best (i.e., lowest energy) approaches for each case. A typical transition state can be seen in Figure 4.

The preference for internal attack was calculated as the free energy difference between the best nucleophilic attack on the terminal and internal position, respectively. For reference, the experimental values in Table 1 correspond to a $\Delta\Delta G_{\text{exp}}^\ddagger = 4 \text{ kJ mol}^{-1}$ for **2a** and -4 kJ mol^{-1} (a preference for terminal attack) for **2b**. The calculated results were found to depend strongly on the actual method used. With a small basis set (method I), both complexes prefer terminal attack; $\Delta\Delta G_{\text{I}}^\ddagger = -2 \text{ kJ mol}^{-1}$ for **2a** and -23 kJ mol^{-1} for **2b**. Employing a larger basis set, method II, yielded a substantially better result for **2a**, $\Delta\Delta G_{\text{II}}^\ddagger = 5 \text{ kJ mol}^{-1}$, in good agreement with the experimental results. For **2b**, the results are still in qualitative agreement with the experimental results, but the absolute preference for terminal attack is strongly exaggerated, 31 kJ mol^{-1} . Interestingly enough, applying a vdW correction (method III) brings the energy difference much closer to the experimental values: $\Delta\Delta G_{\text{III}}^\ddagger = 6 \text{ kJ mol}^{-1}$ for **2a** and -10 kJ mol^{-1} for **2b**. It should be noticed that independent of the method, the trend is correct in that the amount of internal attack decreases when going from short to long tether.

Discussion

The computational studies have been able to reproduce the experimental selectivities with a fair accuracy. However, this does not in itself tell us why the reactivity shifts as a function of the tether length. In order to shed light on the situation, we therefore subjected the structures of **2a** and **2b**, and the transition states resulting from them, to further scrutiny.

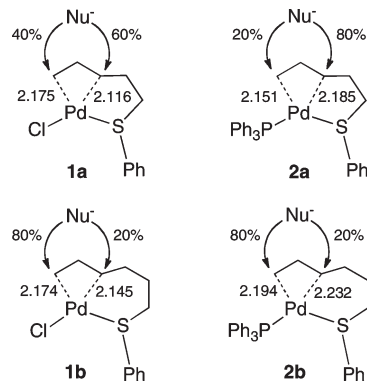


Figure 5. Length of the bonds observed in the X-ray structures versus the regioselectivity in the nucleophilic attack.

Several factors influencing the regioselectivity have been reported in the literature, as outlined in the Introduction. The expected selectivity for nucleophilic attack on a *syn*-monosubstituted (η^3 -allyl)Pd is a strong preference for terminal attack,^{7,8} in reasonable agreement with the results for the long tether (**2b**), but not for the short tether (**2a**). Increased preference for internal attack is found for *anti*-isomers,^{7,8} but this possibility can be excluded in the current case. Only the *syn*-complexes were observed in both solid state and solution, and the computational results also showed a large preference for the *syn*-isomers. Not only were *anti*-isomers prohibitively high in energy, transition state searches for such complexes also revealed that the barriers to nucleophilic attack are high.

Reactivities have also been quantified in terms of the length of the breaking Pd–C bond, the preferred rotation of the η^3 -allyl moiety, and steric hindrance.¹³ In particular, it was found that a longer Pd–C bond corresponds to a more reactive allyl terminus, with each 0.01 Å elongation giving approximately a doubling in reactivity.¹³ We therefore compared the reactivity in the alkylation reaction of the allylic positions in the complexes with the observed bond length in the solid state structures (Figure 5). The calculated structures (in the Supporting Information) showed similar trends.

We can immediately see that the bond lengths detected in the solid state do not give the expected correlation with reactivity. In complex **1a**, the preferred nucleophilic attack occurs on the allylic carbon atom with the shortest Pd–C bond. In complex **2a** the preferred nucleophilic attack was observed at the internal carbon atom, which is the allylic carbon atom with the longest Pd–C bond. Another observation of preferred nucleophilic attack on an allylic carbon with the longest Pd–C bond was in complex **1b**, where a terminal attack was preferred. In complex **2b**, where the longest bond was trans to the donor atom with the expected stronger trans influence (P), the preferred nucleophilic attack was at the other, terminal, carbon atom. In an isodesmic comparison, we can see a modest trans influence, in that bonds trans to P are slightly longer than the corresponding bonds trans to Cl. Thus, Pd–C3 in **2a** is longer than Pd–C3 in **1a**, and the same is true for **2b** versus **1b**. With the shorter tether, there is also a slight increase in the reactivity of the bond trans to P. However, in **2b** the kinetic trans effect is completely absent, in that no change is observed when going from a chloride to phosphine auxiliary ligand, even though there is a significant trans influence.

The calculated bond lengths are similar to those observed in the X-ray structures (Table 3). The Pd–C3 bond in the

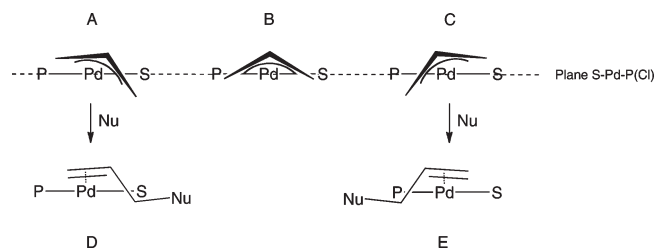


Figure 6. Different orientations of the η^3 -allyl with respect to the S–Pd–P(Cl) plane.

Table 3. Selected Bond Lengths (Å) in the Allylic Moiety for **1a,b** and **2a,b** in the X-ray and Two Lowest Energy DFT Structures for Each Complex

structure	Pd–C1	Pd–C3
1a (X-ray)	2.175(4)	2.116(3)
1a (DFT_1)	2.174	2.155
1a (DFT_2)	2.169	2.156
1b (X-ray)	2.174(8)	2.145(6)
1b (DFT_1)	2.163	2.193
1b (DFT_2)	2.166	2.202
2a (X-ray)	2.151(10)	2.185(9)
2a (DFT_1)	2.220	2.217
2a (DFT_2)	2.215	2.216
2b (X-ray)	2.194(7)	2.232(7)
2b (DFT_1)	2.186	2.290
2b (DFT_2)	2.186	2.300

larger tether, **2b**, is to some extent elongated in the calculated structure, but previous results have shown that similar complexes can give anomalies in the bond trans to phosphorus.²⁹ Overall, the agreement between the DFT structures and the crystallographic data is good (Table 3).

It has also been shown that reactivity can be correlated with the enforced product-like rotation of the (η^3 -allyl)Pd moiety in the ground state.^{13,30} We have measured this rotation as displacements of the two terminal carbons in the η^3 -allyl from the S–Pd–P(or Cl) plane (Figure 6).

Figure 6 shows different ways the η^3 -allyl can orient itself with respect to the S–Pd–P(Cl) plane. The symmetric fashion, represented by situation B in Figure 6, will not induce any product preference. In the other two orientations, A and C, there will be a preferred pathway to form product due to the prerotation of the η^3 -allyl toward one of the two isomeric products.³⁰ In situation A, the internal attack of the nucleophile (trans to P) will be favored, since this orientation of the allylic moiety resembles the coordinated product formed from this attack (structure D in Figure 6). Likewise, situation C resembles the product formed from a terminal attack (trans to S, structure E in Figure 6). In both X-ray and calculated structures (Table 4), the shorter tether has an orientation that resembles situation A and therefore should give a preference for the internal attack. This correlates satisfactorily to the experimental results. In the case of the longer tether, it has a more symmetric orientation (situation B), and it is therefore harder to rationalize the product formation based on the enforced rotation of the allyl.

(29) Hagelin, H.; Åkermark, B.; Norrby, P.-O. *Organometallics* **1999**, *18*, 2884–2895.

(30) (a) Frost, C. G.; Howarth, J.; Williams, J. M. J. *Tetrahedron: Asymmetry* **1992**, *3*, 1089–1122. (b) Reiser, O. *Angew. Chem., Int. Ed. Engl.* **1993**, *32*, 547–549. (c) Peña-Cabrera, E.; Norrby, P.-O.; Sjögren, M.; Vitagliano, A.; deFelice, V.; Oslob, J.; Ishii, S.; Åkermark, B.; Helquist, P. *J. Am. Chem. Soc.* **1996**, *118*, 4299–4313. (d) Dierkes, P.; Ramdeehul, S.; Barloy, L.; De Cian, A.; Fischer, J.; Kamer, P. C. J.; van Leeuwen, P. W. N. M.; Osborn, J. A. *Angew. Chem., Int. Ed.* **1998**, *37*, 3116–3118.

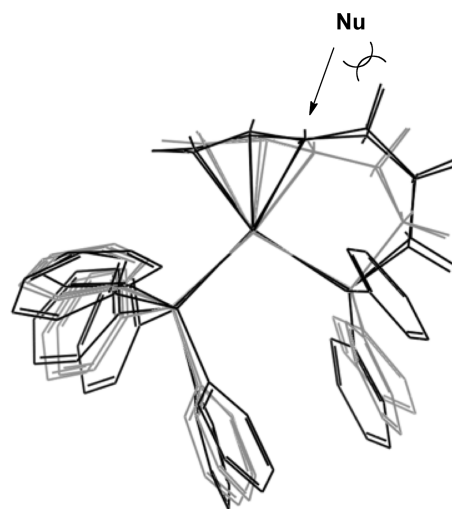


Figure 7. Overlay of two low-energy conformers each of **2a** (gray) and **2b** (black), showing steric interactions with a nucleophile attacking the internal position. Phenyl hydrogens are hidden for clarity.

Table 4. Torsion Angles (deg) of the Allylic Moiety for **1a,b** and **2a,b** in the X-ray and Two Lowest Energy DFT Structures for each Complex

structure	C1 to plane [P(or Cl)–Pd–S] ^a	C3 to plane [P(or Cl)–Pd–S] ^a
1a (X-ray)	0.309	–0.199
1a (DFT_1)	0.144	–0.311
1a (DFT_2)	0.087	–0.121
1b (X-ray)	–0.107	–0.419
1b (DFT_1)	–0.067	–0.330
1b (DFT_2)	–0.294	–0.275
2a (X-ray)	0.072	–0.317
2a (DFT_1)	0.098	–0.268
2a (DFT_2)	0.106	–0.162
2b (X-ray)	–0.116	–0.185
2b (DFT_1)	–0.055	–0.078
2b (DFT_2)	–0.328	–0.607

^a Positive value if situated on the same side of the plane as H2.

Steric factors have been shown to have a strong influence on the relative reactivity of the two termini of the η^3 -allyl. The selectivity in nucleophilic attack has been shown to correlate well with the energy cost of adding a steric probe at a distance of 2.5 Å from the reactive terminus,¹³ close to the position of the nucleophile determined in the current study. A strong indication that vdW interactions could be a determining factor in the current case comes from the observation that it was necessary to apply a vdW correction³¹ to the B3LYP calculations to get more than a qualitative agreement with the experimental results for **2b**, whereas no significant influence was seen for **2a**. When overlaying the lowest energy conformers of the two structures (Figure 7), it is clear that there is a significant difference in the interaction with the incoming nucleophile by the methylene group adjacent to the allylic moiety. The orientation of the tethered substituent in **2b** is similar to the orientation of the substituent found in unstrained *syn*-complexes,³⁰ as expected from the observed selectivity. The tether in **2a** is bent away from the incoming nucleophile, substantially decreasing the steric hindrance at this position, in good agreement with the experimental results.

(31) Grimme, S.; Antony, J.; Ehrlich, S.; Krieg, H. *J. Chem. Phys.* **2010**, *132*, 154104.

Table 5. Average Length of the Forming C–C Bond in Nucleophilic Attack on 2

complex	internal attack distance (Å)	terminal attack distance (Å)
2a	2.31	2.29
2b	2.23	2.26

Analysis of the forming bond lengths in the transition states for attack on **2a** and **2b** confirms the importance of steric repulsion in determining selectivity. In accordance with the general Bell–Evans–Polanyi theory,³² and also with the more specific Hammond postulate,³³ increased steric hindrance should result in a “later” transition state, that is, a shorter forming bond.³⁴ The bond lengths shown in Table 5 confirm that the “earliest” attack is for the internal position in **2a**, with a 0.02 Å shorter forming bond for the terminal position in the same complex. The opposite trend is seen in **2b**, where the forming bond at the internal position is 0.03 Å shorter than the one at the terminal position, indicating significant steric hindrance at the internal position of **2b**, but not **2a**.

Conclusions

Experimental studies of (η^3 -allyl)Pd complexes with tethered ligands indicate that the geometry of the allyl moiety is more important than electronic effects in determining selectivity of nucleophilic attack. However, a weak trans effect on the product selectivity could be observed by varying the nature of the auxiliary ligand.

A computational investigation could reproduce the trend in selectivities using standard DFT methods, but a reasonable quantitative agreement was obtained only when a vdW correction was applied, in agreement with recent studies of organometallic reactivity.³⁵

Several previously suggested factors for controlling regioselectivity in nucleophilic attack on (η^3 -allyl)Pd systems were evaluated in order to rationalize the observed selectivities. These include observable geometric factors such as the length of the Pd–C bond and the ground state rotation of the allyl moiety, as well as interactions with the nucleophile and trans effects from the ligands on Pd. In the current case, a combination of the rotation of the allylic moiety and an important steric repulsion appear to be the dominant factors in determining regioselectivity.

Computational Methods

The different conformations of complexes **1a** and **1b** were generated using a modified MM2 force field²⁰ and used as starting points for further calculations. All structures have been optimized in Jaguar, with the B3LYP hybrid functional³⁶ and the LACVP* basis set.³⁷ The complexes were optimized *in vacuo*

and subjected to vibrational analysis to validate the nature of the stationary points as ground or transition states, respectively. Vibrational contributions to the free energy were calculated at 373.15 K. Solution phase energies were obtained by single-point calculations on the gas phase structure. Solvent was modeled by Jaguar's Poisson–Boltzmann method³⁸ with parameters describing dichloromethane ($\epsilon = 9.08$, probe radius 2.33237 Å); the results are virtually identical with parameters for THF.²⁸ The solution phase Gibbs free energy was estimated by adding the gas phase vibrational contribution to the single-point solution phase energy (method I). Effects of a large basis set were estimated by replacing the potential energies by single-point energies obtained using a larger basis set, LACVP**++ (method II). Starting from method II, the nonbonded interactions were corrected using the approach of Grimme³¹ as a single-point correction (method III).

In the transition state searches the sodium ion was chelated to both carbonyl oxygens of the nucleophilic enolate, forming a relatively rigid six-membered ring (Figure 4). To avoid a non-physical electrostatic collapse in the gas phase calculations, the coordination sphere of sodium was filled with two small solvent models, Me₂O. Initial transition state structures were located by driving the forming C–C bond with 0.1 Å increments and optimizing all other degrees of freedom. All transition states were refined by eigenmode following and verified by the presence of exactly one imaginary frequency. Visual inspection confirmed that the eigenvector corresponded well to the formation of the new C–C bond.

Experimental Section

General Procedures. Products were identified by NMR spectroscopy and GC-MS. ¹H NMR spectra were recorded on a JEOL Eclipse 400 instrument, operating at 400 MHz for the recording of ¹H. Samples were dissolved in CDCl₃, and chemical shifts are given in ppm relative to residual CHCl₃ (7.27 ppm).

GC-MS were run on a Varian 3400 GC with a Varian Saturn 2000 MS, with SB-5 MS columns; helium gas was used as carrier gas. GC were run on a Varian 3900, with CP-SIL 8 CB columns; hydrogen gas was used as carrier gas.

Elemental analyses were performed by Analytische Laboratorien, Gummersbach, Germany.

X-ray diffraction: crystals were mounted on glass needles and transferred to a Rigaku R-Axis IIC image plate system. Diffracted intensities were measured at 293(2) K, using graphite-monochromated Mo K α radiation ($\lambda = 0.71073$ Å) from a Rigaku RU-H3R rotating anode operating at 50 kV and 50 mA. A total of 90 oscillation photos with a rotation angle of 2° were collected. An empirical absorption correction was applied using the REQAB program. The structures were solved using the program SIR-92³⁹ and refined using SHELX-97,⁴⁰ operating in the WinGX program suite.⁴¹ All non-hydrogen atoms were refined anisotropically, and the allylic hydrogen atoms were refined where the data quality so allowed and otherwise included in calculated positions and refined using a riding model. Structures were drawn using ORTEP3⁴¹ for Windows.

All reactions were performed under a nitrogen atmosphere in oven-dried glassware. THF was distilled from Na/benzophenone, and CH₂Cl₂ and pyridine were distilled from CaH₂, all under a nitrogen atmosphere. Commercially available reagents

(32) (a) Bell, R. P. *Proc. R. Soc. London, Ser. A* **1936**, *154*, 414–429. (b) Evans, M. G.; Polanyi, M. *J. Chem. Soc., Faraday Trans.* **1936**, *32*, 1333–1360. (c) For a discussion see: Jensen, F. *Introduction to Computational Chemistry*; Wiley: Chichester, 1999.

(33) Hammond, G. S. *J. Am. Chem. Soc.* **1955**, *77*, 334–338.

(34) Norrby, P.-O. *J. Mol. Struct. (THEOCHEM)* **2000**, *506*, 9–16.

(35) Averkiev, B. B.; Zhao, Y.; Truhlar, D. G. *J. Mol. Catal. A* **2010**, *324*, 80–88.

(36) (a) Becke, A. D. *Phys. Rev. A* **1988**, *38*, 3098–3100. (b) Lee, C. T.; Yang, W. T.; Parr, R. G. *Phys. Rev. B* **1988**, *37*, 785–789. (c) Stephens, P. J.; Devlin, F. J.; Chabalowski, C. F.; Frisch, M. J. *J. Phys. Chem.* **1994**, *98*, 11623–11627.

(37) LACVP basis sets use 6-31G for main group elements, and the Hay-Wadt ECP for Pd: Hay, P. J.; Wadt, W. R. *J. Chem. Phys.* **1985**, *82*, 299–310.

(38) (a) Tannor, D. J.; Marten, B.; Murphy, R.; Friesner, R. A.; Sitkoff, D.; Nicholls, A.; Ringnalda, M.; Goddard, W. A., III; Honig, B. *J. Am. Chem. Soc.* **1994**, *116*, 11875–11882. (b) Marten, B.; Kim, K.; Cortis, C.; Friesner, R. A.; Murphy, R. B.; Ringnalda, M. N.; Sitkoff, D.; Honig, B. *J. Phys. Chem.* **1996**, *100*, 11775–11788.

(39) Altomare, A.; Cascarano, G.; Giacovazzo, C.; Gualardi, A. *J. Appl. Crystallogr.* **1993**, *26*, 343–350.

(40) Sheldrick, G. M. *Acta Crystallogr.* **2008**, *A64*, 112–122.

(41) (a) Farrugia, L. J. *J. Appl. Crystallogr.* **1999**, *32*, 837–838. (b) Farrugia, L. J. *J. Appl. Crystallogr.* **1997**, *30*, 565.

were used as delivered unless stated otherwise. TLC was performed using alumina plates coated with silica gel 60, F₂₅₄. The plates were visualized by using a mixture of 2% KMnO₄ and 4% K₂CO₃(aq) followed by warming with a heat gun, which resulted in yellow spots. Column chromatography was performed using silica gel 60, 0.04–0.06 mm.

6-(Phenylthio)hex-1-ene. Thiophenol (2.0 mL, 15 mmol) was added to a degassed solution of NaOH (0.9 g, 22.5 mmol, in 3 mL of H₂O), under a N₂ atmosphere. The solution was stirred for 30 min, until it had reached room temperature. Thereafter 6-bromo-1-hexene (1.34 mL, 10 mmol) was added dropwise. The reaction mixture was stirred at room temperature under N₂ for 16 h. The product was extracted with Et₂O (3 × 15 mL) and then washed with H₂O (15 mL) and brine (15 mL) and dried with Na₂SO₄. After evaporation of the solvent, the crude product was collected as a light yellow oil (1.89 g, 9.8 mmol, 98%). ¹H NMR (400 MHz, CDCl₃): δ (ppm) 7.24–7.25 (m, 4H), 7.13–7.20 (m, 1H), 5.0 (dm, 1H), 4.95 (dm, 1H), 2.92 (t, 2H), 2.07 (app. q, 2H), 1.67 (app. p, 2H), 1.53 (app. p, 2H).

5-(Phenylthio)pent-1-ene. As previous (1.68 g, 9.5 mmol, 95%). ¹H NMR (400 MHz, CDCl₃): δ (ppm) 7.24–7.34 (m, 4H), 7.13–7.20 (m, 1H), 5.72–5.84 (m, 1H), 5.04 (dm, 1H), 4.98 (dm, 1H), 2.92 (br t, 2H), 2.19 (app. br q, 2H), 1.74 (app. p, 2H).

Chloro(*syn*-5-phenylthiopent(1–3- η)-enyl)palladium (1a). 5-(Phenylthio)pent-1-ene (178 mg, 1.0 mmol) was dissolved in THF (2 mL, dry), and Pd(OCOCF₃)₂ (332 mg, 1.0 mmol) was added together with 2 mL of dry THF, and the deep red solution was stirred for 30 min, under N₂. DIPEA (175 μ L, 1.0 mmol) was added dropwise, and LiCl (47 mg, 1.1 mmol) was added after 5 min. The black solution was stirred for 20 min; then the solvent was evaporated and the black residue was redissolved in CH₂Cl₂ and filtered through a Pasteur pipet with Celite. The crude product was purified by flash chromatography (CH₂Cl₂/MeOH, 20:1) and thereafter recrystallized from CH₂Cl₂/Et₂O, yielding the product as light yellow needles (0.140 mg, 0.44 mmol, 44%). ¹H NMR (400 MHz, CDCl₃): δ (ppm) 7.77–7.82 (m, 2H), 7.32–7.44 (m, 3H), 5.72–5.81 (m, 1H), 4.30 (dt, 1H), 4.16 (dd, 1H), 3.86 (ddd, 1H), 3.64 (dt, 1H), 3.15 (app. d, 1H), 1.99–2.15 (m, 2H). Anal. Calcd for C₁₁H₁₃ClPdS: C, 41.40; H, 4.11. Found: C, 41.23; H, 3.99.

Chloro(*syn*-6-phenylthiohex(1–3- η)-enyl)palladium (1b). 6-(Phenylthio)hex-1-ene (1.0 mmol, 192 mg) was dissolved in dry THF (3 mL), and Pd(OCOCF₃)₂ (1.0 mmol, 332 mg) was added together with 2 mL of dry THF. Directly after, NaHCO₃ (252 mg, 3 mmol) was added, under N₂. The solution went from deep red to almost black. The reaction was stirred for 16 h. LiCl (63.6 mg, 1.5 mmol) was added, and after 20 min the solvent was evaporated and the black residue was redissolved in CH₂Cl₂ and filtered through a Pasteur pipet with Celite. The crude product was purified by flash chromatography (CH₂Cl₂/MeOH, 20:1), yielding the product as a crystalline foam (0.096 mg, 0.29 mmol, 29%). A small sample was recrystallized from CH₂Cl₂/Et₂O, which gave the product as orange crystals. ¹H NMR (400 MHz, CDCl₃): δ (ppm) 7.80–7.85 (m, 2H), 7.36–7.42 (m, 3H), 5.17–5.28 (m, 1H), 4.42 (dd, 1H), 3.45 (dt, 1H), 3.36 (app. d, 1H), 3.16 (app. ddd, 1H), 2.25–2.41 (m, 2H), 2.27 (dt, 1H), 1.61–1.74 (app. q, 1H), 1.45–1.57 (br q, 1H). Anal. Calcd for C₁₂H₁₅ClPdS: C, 43.26; H, 4.54. Found: C, 43.18; H, 4.41.

(*syn*-5-Phenylthiopent(1–3- η)-enyl)(triphenylphosphine)palladium Tetrafluoroborate (2a). The chloro complex 1a (191 mg, 0.6 mmol) was dissolved in dry CH₂Cl₂ (4 mL) under a N₂ atmosphere and added to PPh₃ in dry CH₂Cl₂ (1 mL). After 5 min, AgBF₄ (126.5 mg, 0.65 mmol) was added to the solution and rinsed down with dry CH₂Cl₂ (2 mL). The solution was

evacuated and refilled with N₂ two times and then stirred for 1 h. The formed precipitate was filtered off through a Pasteur pipet with Celite, and after evaporation of the solvent the product was collected as a bright yellow crystalline foam (367 mg, 0.58 mmol, 97%). A small sample was recrystallized from CH₂Cl₂/Et₂O, which gave the product as light yellow needles. ¹H NMR (400 MHz, CDCl₃): δ (ppm) 7.32–7.44 (m, 10H), 7.23–7.31 (m, 8H), 7.16–7.22 (m, 2H), 6.20–6.30 (app. sextet, 1H), 5.74–5.84 (m, 1H), 4.24–4.33 (app. dt, 1H), 4.05 (app. d, 1H), 4.00 (dd, 1H), 3.57 (app. d, 1H), 2.47–2.58 (m, 1H), 2.32–2–45 (m, 1H). Anal. Calcd for C₂₉H₂₈BF₄PPdS: C, 55.04; H, 4.46. Found: C, 54.91; H, 4.60.

(*syn*-6-Phenylthiohex(1–3- η)-enyl)(triphenylphosphine)palladium Tetrafluoroborate (2b). As 2a, but starting from 1b (57 mg, 0.17 mmol), yielding the product as a light yellow foam (108 mg, 0.167 mmol, 98%). A small sample was recrystallized from CH₂Cl₂/Et₂O, which gave the product as light yellow needles. ¹H NMR (400 MHz, CDCl₃): δ (ppm) 7.17–7.43 (m, 20H), 5.78 (dt, 1H), 5.48 (m, 1H), 4.18 (br d, 1H), 3.30 (br d, 1H), 2.92 (m, 1H), 2.69–2.82 (m, 1H), 2.47 (br d, 1H), 2.25–2.35 (m, 1H), 2.12 (br q, 1H), 1.72 (br q, 1H). Anal. Calcd for C₃₀H₃₀BF₄PPdS: C, 55.71; H, 4.68. Found: C, 55.58; H, 4.66.

General Procedure for the Allylic Alkylation. NaH (6 mg, 0.15 mmol, 60% suspension in oil) was suspended in dry THF (1 mL), and the flask was evacuated and refilled with N₂. Dimethyl malonate (0.15 mmol, 17 μ L) was added dropwise to the suspension, which turned clear after the addition. The solution was stirred at room temperature for 10 min.

The malonate solution was added to the palladium complex (0.1 mmol) in dry CH₂Cl₂ (1 mL) under a N₂ atmosphere. The reaction mixture was stirred for 3 h, then diluted with Et₂O (5 mL) and washed with HCl (1M, 3 mL), H₂O (5 mL), and brine (5 mL). The organic solution was dried over Na₂SO₄ and filtrated through Celite, and the crude product mixture was analyzed by GC-MS and ¹H NMR. For further analysis the products (4a,b and 5a, except 5b due to low yield) were purified by column chromatography using EtOAc/pentane (1:5). The analyses were in agreement with the previously reported structures.²³

Dimethyl 2-(5-(Phenylthio)pent-2-en-1yl)malonate (4a). ¹H NMR (400 MHz, CDCl₃): δ (ppm) 7.24–7.34 (m, 4H), 7.15–7.20 (m, 1H), 5.52–5.62 (m, 1H), 5.39–5.48 (m, 1H), 3.74 (s, 6H), 3.42 (t, 1H), 2.91 (t, 2H), 2.60 (app. t, 2H), 2.31 (app. q, 2H).

Dimethyl 2-(6-(Phenylthio)pent-2-en-1yl)malonate (4b). ¹H NMR (400 MHz, CDCl₃): δ (ppm) 7.24–7.34 (m, 4H), 7.13–7.20 (m, 1H), 5.35–5.56 (m, 2H), 3.72 (s, 6H), 3.41 (t, 1H), 2.88 (t, 2H), 2.58 (app. t, 2H), 2.12 (app. q, 2H), 1.67 (app. p, 2H).

Dimethyl 2-(5-(phenylthio)pent-1-en-3yl)malonate (5a). ¹H NMR (400 MHz, CDCl₃): δ (ppm) 7.24–7.34 (m, 4H), 7.13–7.20 (m, 1H), 5.58–5.69 (m, 1H), 5.12–5.19 (m, 2H), 3.67 (s, 3H), 3.67 (s, 3H), 3.39 (d, 1H), 2.91–3.02 (m, 2H), 2.75–2.84 (m, 1H), 1.73–1.83 (m, 1H), 1.59–1.71 (m, 1H).

Acknowledgment. The Swedish Research Council is gratefully acknowledged for support. We want to thank Professors Paul Helquist and Aldo Vitagliano for valuable input in the early phase of the project.

Supporting Information Available: This material is available free of charge via the Internet at <http://pubs.acs.org>.